Conference on Modelling Fluid Flow (CMFF'25)
The 19th International Conference on Fluid Flow Technologies
Budapest, Hungary, August 26-August 29, 2025

Equilibrium Positions and Dynamic behavior of Thermal Prolate Particles in Shear Flow: Influence of Particle Size

Farshad GHARIBI[1], Dominique THÉVENIN[2]

[1] Corresponding Author. Laboratory of Fluid Dynamics and Technical Flows, University of Magdeburg "Otto von Guericke", D-39106 Magdeburg, Germany, E-mail: farshad.gharibi@ovgu.de
[2] Laboratory of Fluid Dynamics and Technical Flows, University of Magdeburg "Otto von Guericke", E-mail: Thevenin@ovgu.de

ABSTRACT

An accurate characterization of the trajectory and dynamic behavior of particles is crucial for processes such as particle manipulation, design of efficient heating and cooling mechanisms, pollutant dispersion, and biomedical applications. Despite significant progress in the simulation of particle-fluid interactions, the dynamics of non-spherical particles, especially when heat transfer is considered, is still an active area of research. The focus of this study is on prolate particles in shear flows using four-way direct numerical simulation (DNS). For this purpose, we employ a hybrid computational framework, in which the lattice Boltzmann method is used for simulating the fluid flow, the finite-difference approach for solving the energy equation, the immersed boundary method (IBM) to capture fluid-particle interactions and the Discrete Element Method (DEM) for modeling particle collisions. This enables us to accurately model the behavior of particles under isothermal and non-isothermal conditions while varying particle size. The effect of heat transfer on final equilibrium position and dynamic behavior of prolate particles in shear flows are computed and analyzed. The results indicate that the confinement ratio, defined as the ratio of particle major radius to channel width, has a significant impact on both the time it takes for a particle to reach its equilibrium position and the vertical location of that position.

Keywords: Lattice Boltzmann method, Particulate flow, Prolate particle, Shear flow

1. INTRODUCTION

Understanding particle behavior in fluid flows is fundamentally important for a broad spectrum of industrial, environmental, and biological applications. The investigation of particle migration under varying flow conditions is essential for advancing the understanding of particulate motion in complex fluid environments. Given that particles in real-world applications often deviate from idealized spherical geometries, a detailed investigation into the dynamics of non-spherical particles is essential for enhancing the predictive accuracy and applicability of particle-laden flow models. The dynamics of spheroidal particles suspended in shear flows have long been a subject of fundamental research in fluid mechanics. Jeffery [1] already provided an analytical description of the rotational kinematics of isolated spheroidal particles immersed in a viscous fluid under linear shear conditions, assuming negligible inertial effects corresponding to the limit of zero particle Reynolds number. While analytical methods are generally constrained to simplified flow configurations, direct numerical simulations enable the exploration of a broader spectrum of physical phenomena in diverse flow regimes. However, with increasing fluid inertia, the symmetry of the flow field surrounding the particle is broken, giving rise to more intricate and nonlinear particle dynamics. Fox et al. [2] conducted a study on spherical particles in inertia-dominated shear flows and identified a supercritical pitchfork bifurcation occurring beyond a critical particle Reynolds number (Re_p), resulting in the stabilization of two symmetric off-center equilibrium positions. More recently, Lauricella et al. [3] demonstrated that ellipsoidal particles exhibit distinct behavior, tending to return to the centerline at elevated Re_p, in contrast to spherical particles, which display instability under similar conditions. In our previous work [4], we studied the dynamic behavior of a thermal spheroidal particle with fixed size in shear flows. The present study investigates the influence of particle size on the dynamic behavior of thermal non-spherical particles. Such insights may serve as a foundational step toward the development of novel techniques for the thermal and hydrodynamic manipulation of particles. The lattice Boltzmann method (LBM) has emerged as a widely adopted computational framework for simulating fluid flow systems in-

volving particulate suspensions [2, 5, 6]. In the present study, a hybrid computational framework is utilized, combining LBM for fluid flow, Finite-Difference (FD) schemes for the thermal field, the Immersed Boundary (IB) method for fluid–structure interaction, and the Discrete Element Method (DEM) for modeling particle dynamics and collisions. This integrated approach enables high-fidelity simulations of coupled fluid-particle-thermal interactions. All simulations are carried out using the extensively validated in-house solver ALBORZ [7].

2. NUMERICAL METHODS

Employing the LBM, this study conducts flow field simulations. Using a finite-order spectral method with Hermite polynomials, the Boltzmann equation is discretized in phase space. The ensuing system of interconnected hyperbolic equations is resolved by integrating along the characteristics, yielding the "stream-collide" equation for discrete populations f_i:

$$f_i(\mathbf{x} + \mathbf{e}_i\delta t, t + \delta t) = f_i(\mathbf{x}, t) + \Omega_i + F_i^{ext}, \tag{1}$$

where $\mathbf{x}$ represents the fluid node's spatial location, t denotes time, F_i^{ext} describes the external forces, and $\mathbf{e}_i$ corresponds to the discrete velocity vectors, determined based on the lattice structure chosen, and $\mathbf{e}_i\delta t$ denotes the positional shift in different directions. Throughout this investigation, the focus will be exclusively set on the D3Q27 stencil. In Equation (1), Ω_i is the discrete collision operator. In this study, a modified Hermite central moments space collision operator is utilized, which allows to control bulk viscosity independently. Unlike the traditional Hermite polynomial space, this modified formulation allows for the independent relaxation of trace-free and trace components of the second order moments,

$$\Omega_i = \mathcal{T}^{-1} S \mathcal{T}(f_i^{eq} - f_i) + E_i, \tag{2}$$

where S corresponds to the diagonal matrix of the relaxation rates, $\mathcal{T}$ represents the transform tensor for moments, while $\mathcal{T}^{-1}$ represents its inverse, which are determined based on the set of Hermite polynomials. In Equation (2), f_i^{eq} is the discrete equilibrium distribution. The equilibrium distribution function in discrete form is determined through an expansion at a given reference temperature of the Maxwell-Boltzmann distribution, equivalently reference isothermal speed of sound c_s, via Hermite polynomials. The expansion allows then the use of the Gauss-Hermite quadrature to satisfy exact recovery of the desired number of moments of the distribution function on the selected set of discrete velocity vectors leading to:

$$f_i^{eq} = w_i \sum_{n=0}^{N} \frac{1}{n! c_s^{2n}} H_n(\mathbf{e}_i) : a_n^{eq}\left(\rho, \mathbf{u}, \frac{p}{\rho}\right), \tag{3}$$

where ":" represents the Frobenius inner product and w_i represents the lattice weight factor based on Equation (4) for three-dimensional cases. H_n denotes the Hermite polynomial tensor of rank n. The quantity a_n^{eq} is the corresponding equilibrium Hermite coefficient, $\mathbf{u}$ corresponds to velocity, p signifies pressure, ρ represents fluid density, and N indicates the expansion order.

$$\begin{aligned} w_i = \{ & w_0 = \frac{8}{27}, w_{1-6} = \frac{2}{27}, w_{7-18} = \frac{1}{54}, \\ & w_{19-26} = \frac{1}{216} \} \end{aligned} \tag{4}$$

In Equation (2), E_i is a term that takes into account for variations in the diagonal elements of the equilibrium third-order moments [6]. This term ensures that Galilean invariance is maintained in the discretized representation. In fact, the lack of independent support for diagonal terms in third-order moments by standard lattices causes viscosity to exhibit an unconventional dependence on fluid velocity, i.e., non-Galilean-invariant (GI) viscous stress. Defined as follows, the moments transformation tensor $\mathcal{T}$ is constructed using a series of modified central Hermite polynomials:

$$\mathcal{T} = [|\overline{\mathcal{T}}_0\rangle, ..., |\overline{\mathcal{T}}_N\rangle], \tag{5}$$

where column vectors $|\overline{\mathcal{T}}_i\rangle$ are based on Hermite polynomials.

The energy equation for incompressible flows but variable properties, when disregarding viscous heating, can be simplified to:

$$\frac{\partial(\rho C_p T)}{\partial t} + \nabla.(\mathbf{u}\, \rho C_p T) = \nabla.(k \nabla T) + Q, \tag{6}$$

in which T denotes temperature, k signifies thermal conductivity, C_p represents the specific heat capacity, and Q represents the heat source term. A Finite-Difference (FD) technique is employed here for solving the energy equation. The third-order WENO approach is employed for discretizing the advection term in the energy equation, ensuring stability even in regions with large gradients. For handling the diffusion terms, a fourth-order central finite difference (FD) scheme is used for spatial discretization, while a first-order explicit Euler discretization is applied in time to update the relevant fields. The term for buoyancy force ($\mathbf{F}_B$) within the flow-field equation is computed using the Boussinesq approximation in this investigation. This approximation assumes a linear relationship between the buoyancy term and the temperature difference. As a result, the momentum and energy relations become coupled, as expressed by:

$$\mathbf{F}_B = \rho_{f,0} \mathbf{g} \beta (T - T_0), \tag{7}$$

The thermal expansion coefficient β, reference temperature T_0, gravity acceleration $\mathbf{g}$, and fluid density at the specified reference temperature $\rho_{f,0}$ appear in this equation. The Exact Difference Method (EDM) force scheme is used to incorporate the bulk forces $\mathbf{F}$ and buoyancy force $\mathbf{F}_B$ arising from particle-fluid interaction through IBM into Equation (1). The Grashof number, defined in Eq. (8), quantifies buoyancy in

relation to viscosity

$$\mathrm{Gr} = \frac{\rho_f^2 \, g \, \beta \, D_p^3 \Delta T}{\mu^2}, \tag{8}$$

In this study, the Direct-Force IBM is employed to represent the fluid-particle interaction forces including heat transfer. Following the approach introduced by Uhlmann [8] and later extended to thermal IBM by [9], the force term ($\mathbf{F}_b$) at each Lagrangian node ($\mathbf{X}_b$) is computed based on the desired velocity ($\mathbf{U}^d$), as outlined in Equation (9). At each Lagrangian node, the heat source term (Q_b^n) is computed using the same way based on the desired particle temperature (T_p^d) using Equation (10):

$$\mathbf{F}_b^n = \frac{\mathbf{U}^d - \mathbf{U}^{noF}}{\Delta t}, \tag{9}$$

$$Q_b^n = \frac{T_p^d - T^{noH}}{\Delta t}, \tag{10}$$

in which Δt is the time step, n denotes current time step, and $\mathbf{U}^{noF}$ denotes the velocity at next time step that would be calculated in the absence of any external forcing (*noF*, for no forcing). For simulations conducted in three dimensions, the computation of $\mathbf{U}^{noF}$ is based on Equation (11), relying on velocity values at Eulerian points ($\mathbf{u}_{i,j,k}$).

In the same way, regarding heat source term computations at each Lagrangian node, the "no heat source" temperature T^{noH} can be calculated using Equation (12) according to the temperature at the Eulerian points ($T_{i,j,k}$). This leads finally to:

$$\mathbf{U}^{noF} = \sum_{i,j,k} \mathbf{u}_{i,j,k} \, D\left(\mathbf{x}_{i,j,k} - \mathbf{X}_b\right) (\Delta h)^3, \tag{11}$$

$$T^{noH} = \sum_{i,j,k} T_{i,j,k} \, D\left(\mathbf{x}_{i,j,k} - \mathbf{X}_b\right) (\Delta h)^3. \tag{12}$$

Here, $\mathbf{x}_{i,j,k}$ is the Eulerian nodes' position, the lattice size is denoted by Δh, and $\mathbf{X}_b$ indicates the Lagrangian points' position. The discretized Dirac delta function (D) is calculated using the 4-point delta function, as proposed by Peskin [10].

The force applied to each Eulerian node and the heat source on the Eulerian nodes can be determined using Equations (13) and (14).

$$\mathbf{F}_{i,j,k} = \rho_f \sum_{\mathbf{b,n}} \mathbf{F}_b^n \, D\left(\mathbf{x}_{i,j,k} - \mathbf{X}_b\right) \, \Delta V_b, \tag{13}$$

$$Q_{i,j,k} = \rho_f C_{p,f} \sum_{\mathbf{b,n}} Q_b^n \, D\left(\mathbf{x}_{i,j,k} - \mathbf{X}_b\right) \, \Delta V_b, \tag{14}$$

where ΔV_b represents the unit volume of the relevant Lagrangian boundary point segment. To incorporate the particle forces into the LBM, the force $F_{i,j,k}$ is added to Equation (1) using EDM force scheme; to incorporate the particles heat source term into the FD solver, the heat source $Q_{i,j,k}$ is included in Equation (6).

At each Lagrangian point, the desired velocity $\mathbf{U}^d$ is formulated as follows:

$$\mathbf{U}^d = \mathbf{U}_p + \Omega_p \times (\mathbf{X}_b - \mathbf{X}_c), \tag{15}$$

where $\mathbf{X}_c$ represents the particle center, and Ω_p and $\mathbf{U}_p$ denote the particle angular and translational velocities, respectively. By applying the fundamental laws of motion, both velocities can be updated using Equations (16) and (17):

$$M_p \frac{d\mathbf{U}_p}{dt} = -\int \mathbf{F}_b dV + M_f \frac{d\mathbf{U}_p}{dt} + (\rho_p - \rho_f) V_p \mathbf{g} + \mathbf{F}^c, \tag{16}$$

$$\mathbf{T} = I \frac{d\Omega_p}{dt} + \Omega_p \times I\Omega_p, \tag{17}$$

where the subscripts "p" indicate particle properties, while "f" refers to fluid properties. The quantity $\mathbf{F}^c$ is the summation of particle–particle and wall-particle collision forces, M represents the mass, I stands for the moment of inertia and $\mathbf{T}$ denotes the total torque experienced by the particle's center.

In the case of heat transfer, for a particle considered as being at a given temperature, one can directly set the values of T_p^d. Otherwise, for particles with varying temperature, the exchanged heat (in the following example, a heat generation Q_p^g) is added to Equation (10):

$$Q_b^n = \frac{T_p^d - T^{noH}}{\Delta t} + Q_p^g. \tag{18}$$

In this study, the contact interactions between particles are modeled using the soft-sphere Discrete Element Method (DEM), wherein the contact forces are computed based on the overlap between interacting particles. The total collision force consists of both normal and tangential components, each derived according to Hertzian contact mechanics [11]. The normal contact force between particle i and particle j is given by:

$$\mathbf{F}_{n,ij} = -k_n \, \delta_n \, \mathbf{n}_{ij} - \eta_n \, \Delta \mathbf{v}_{n,ij}, \tag{19}$$

where, k_n is the normal stiffness coefficient and is considered to be $8 \times 10^4 \frac{N}{m}$ in this work, δ_n is the overlap distance in the normal direction, η_n is the normal damping coefficient and is considered to be $10^2 \frac{kg}{s}$, $\Delta \mathbf{v}_{n,ij}$ is the relative normal velocity between particles. The tangential contact force, based on the Mindlin-Deresiewicz [12] model, is computed as:

$$\mathbf{F}_{t,ij} = -k_t \, \delta_t \, \mathbf{t}_{ij} - \eta_t \, \Delta \mathbf{v}_{t,ij}, \tag{20}$$

where, k_t is the tangential stiffness coefficient and is set to $4 \times 10^4 \frac{N}{m}$, δ_t is the integrated tangential displacement over the contact duration, η_t is the tangential damping coefficient and is considered to be $50 \frac{kg}{s}$, $\Delta \mathbf{v}_{t,ij}$ is the relative tangential velocity between particles.

To ensure consistency with physical frictional lim-

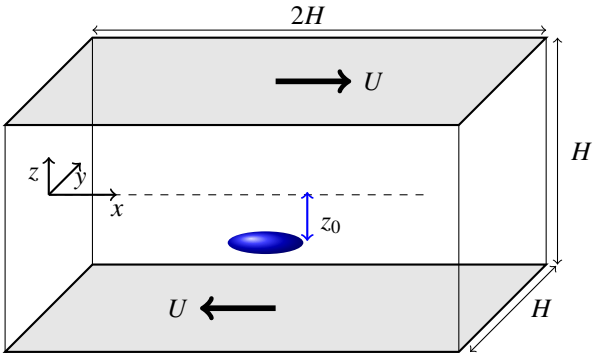

Figure 1. Illustration of the computational domain.

its, the tangential force is bounded by the Coulomb friction criterion:

$$|\mathbf{F}_{t,ij}| \leq \mu_{ij}|\mathbf{F}_{n,ij}|, \tag{21}$$

where μ_{ij} is the coefficient of friction between particles i and j.

3. RESULT

In the present investigation, we examine the flow behavior between two parallel plates moving in opposite directions, each with a constant velocity U, as depicted in Figure 1. The separation distance between the plates is denoted by H, and the computational domain is defined with dimensions $2H \times H \times H$, such that the flow direction extends twice the length of the transverse dimensions. The velocity of the fluid at the walls satisfies the no-slip condition, while periodic boundary conditions are imposed along the remaining directions of the domain.

The suspended particle under consideration is a thermally active prolate spheroid, characterized by a major radius a and a minor radius b. The particle's aspect ratio is defined as $r = a/b$, and its degree of spatial confinement within the channel is quantified using the confinement ratio $K = a/H$. The shear rate for the considered geometry is defined as

$$G = \frac{2U}{H}, \tag{22}$$

To analyze particle dynamics within the flow, we consider a particle initially positioned at (x_0, y_0, z_0) in the computational domain. The particle Reynolds number, using the major radius a as the characteristic length scale, is expressed as:

$$\mathrm{Re}_p = \frac{Ga^2}{\nu}, \tag{23}$$

where ν denotes the kinematic viscosity of the fluid.In this study, a particle Reynolds number of $\mathrm{Re}_p = 30$ is considered for all cases.

This study aims to investigate the influence of the confinement ratio on the equilibrium lateral position of the heated prolate particle in the shear-driven flow. Figure 2 illustrates the migration trajectory of a neutrally buoyant prolate spheroidal particle, initially positioned at $z_0^* = z_0/H = -0.1$, in an isothermal Couette flow. In this scenario, the balance among hydrodynamic forces, inertial lift and wall-induced interactions drives the particle toward a stable vertical equilibrium position near the lower wall. Particles with lower confinement ratios (i.e., smaller relative size compared to the channel height) tend to take longer to reach this equilibrium, which itself occurs at a lower vertical position due to altered balance of forces.

Next, the particle is assumed to be hot with a constant temperature, and a Dirichlet boundary condition—set to the same temperature as the initial fluid domain—is applied on the moving plates. When thermal effects are introduced, as shown in Figure 3 for a thermal case with $\mathrm{Gr} = 80$, the presence of heat transfer significantly alters the particle's equilibrium behavior. In the case with a Grashof number $\mathrm{Gr} = 80$, the thermally induced drag forces arising from buoyancy-driven convection dominate over gravity and other hydrodynamic contributions. As a result, the particle stabilizes in the upper region of the channel. Interestingly, decreasing the confinement ratio in the thermally active case leads to an increase in the final equilibrium height, bringing the particle closer to the upper wall. This behavior indicates a stronger influence of convective forces in less confined environments.

To examine the influence of neighboring particles on the migration dynamics and equilibrium positioning of a heated particle, a configuration of eight particles with aspect ratio $K = 0.1$ is considered. With this consideration, the packing ratio—i.e., the ratio of particle volume to total volume—is equal to 0.004. All particles are initially positioned at $z_0^* = -0.1$, but have different initial streamwise locations x_0 within the domain, with a center-to-center distance of $2.5a$. by th Figure 4 presents the time evolution of the normalized vertical position $z^* = z/H$ for eight thermally active prolate spheroidal particles. The trajectories labeled P0 through P7 correspond to individual particles, while the curve labeled *Mean* represents the ensemble averaged position over time.

Initially, all particles undergo a transient migration phase, during which they move from their initial positions toward a stable equilibrium location. This transient period is most pronounced for $T^* < 50$, reflecting rapid vertical displacement primarily driven by the dominance of convective drag forces in the early stages.

As reported earlier for the single-particle case, the vertical position eventually stabilizes near $z^* \approx 0.4$. However, the presence of multiple particles introduces considerable fluctuations around this equilibrium height. These deviations are attributed to hydrodynamic interactions and flow disturbances caused by neighboring particles. Nevertheless, the mean trajectory converges to a steady-state position similar to the single-particle case, with reducing fluctuations at later times.

Based on the simulation results, the time-averaged

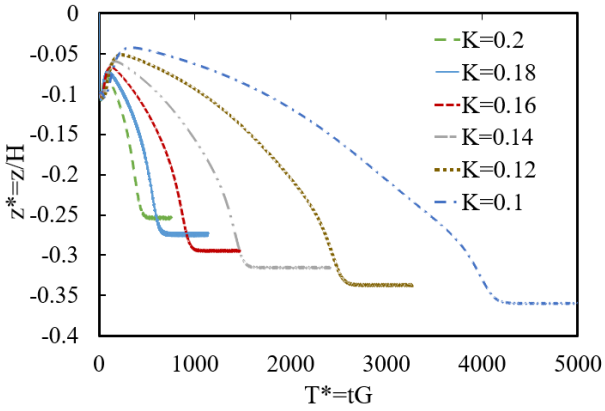

Figure 2. Migration trajectory of an isothermal prolate particle vs. dimensionless time (Gt) at various confinement ratios.

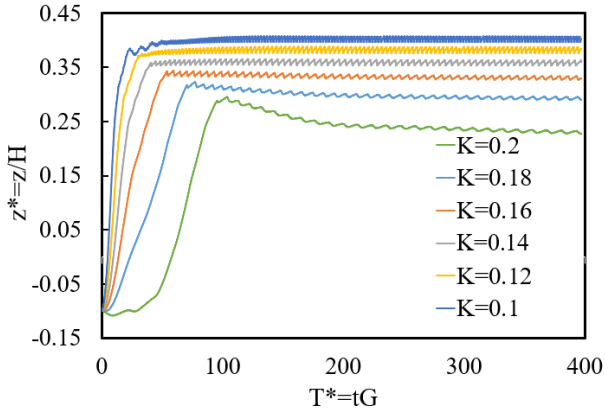

Figure 3. Migration trajectory of a hot prolate particle vs. dimensionless time (Gt) at various confinement ratios for Gr=80.

center-to-center nearest neighbor distance is approximately 3a. The increased fluctuation amplitude observed in the multi-particle case highlights the transient influence of inter-particle interactions, although the long-term equilibrium behavior remains qualitatively consistent with that of single particle. how ever that such behavior may change significantly at higher packing fractions. However, it is important to note that this behavior may change significantly at higher packing fractions.

4. CONCLUSION

In this study, we employed a hybrid computational framework combining the Lattice Boltzmann Method (LBM), Immersed Boundary Method (IBM), a finite-difference (FD) scheme, and the Discrete Element Method (DEM) to investigate the dynamic behavior of non-spherical particles in a shear-driven flow. The results reveal that the confinement ratio significantly influences both the time required for a particle to reach its equilibrium position and the vertical location of that position.

In the isothermal case, particles with lower confinement ratios (i.e., smaller particles relative to the channel height) migrate more slowly toward their equilibrium positions compared to larger particles. Conversely, in the thermal case, smaller particles reach equilibrium more quickly, suggesting that thermally induced forces accelerate vertical migration.

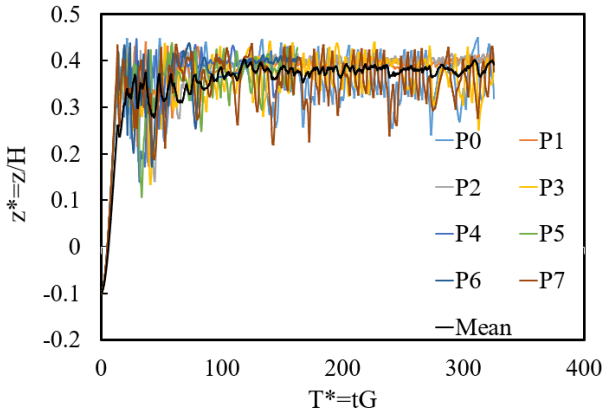

Figure 4. Migration trajectory of eight hot prolate particle vs. dimensionless time (Gt) at confinement ratio K=0.1 for Gr=80.

Furthermore, in both isothermal and thermal configurations, particles with lower confinement ratios tend to equilibrate farther from the channel centerline. The presence of multiple particles within the domain introduces complex interactions. Particle-particle collisions, coupled with hydrodynamic interactions and flow disturbances, lead to chaotic fluctuations in the vertical equilibrium positions. However the mean trajectory position is consistent with that of single particle.

5. ACKNOWLEDGEMENTS

The authors gratefully acknowledge funding by the Deutsche Forschungsgemeinschaft (DFG, German Research Foundation) within Project number 465872891. Also, the authors gratefully acknowledge the Gauss Centre for Supercomputing e.V. (www.gauss-centre.eu) for funding this project by providing computing time on the GCS Supercomputer [HAWK| HUNTER] at Höchstleistungsrechenzentrum Stuttgart (www.hlrs.de)

REFERENCES

[1] Jeffery, G. B., 1922, "The motion of ellipsoidal particles immersed in a viscous fluid", *Proceedings of the Royal Society of London Series A, Containing papers of a mathematical and physical character*, Vol. 102 (715), pp. 161–179.

[2] Fox, A. J., Schneider, J. W., and Khair, A. S., 2021, "Dynamics of a sphere in inertial shear flow between parallel walls", *Journal of Fluid Mechanics*, Vol. 915, p. A119.

[3] Lauricella, G., Naderi, M. M., Zhou, J., Papautsky, I., and Peng, Z., 2024, "Bifurcation of equilibrium positions for ellipsoidal particles in iner-

tial shear flows between two walls", *Journal of Fluid Mechanics*, Vol. 984, p. A47.

[4] Gharibi, F., Fard, A. E., and Thévenin, D., 2025, "Dynamic behaviour of a thermal spheroid particle in shear flows", *Journal of Fluid Mechanics*, Vol. 1013, p. A40.

[5] Khalili, B., Rahnama, M., Jafari, S., Gharibi, F., and Jahanshahi Javaran, E., 2017, "Lattice Boltzmann simulation of solid particles motion in a three dimensional flow using smoothed profile method", *Journal of Applied Fluid Mechanics*, Vol. 10 (4), pp. 1091–1103.

[6] Gharibi, F., Hosseini, S. A., and Thévenin, D., 2024, "A hybrid lattice Boltzmann/immersed boundary method/finite-difference model for thermal fluid-solid interactions", *International Communications in Heat and Mass Transfer*, Vol. 155, p. 107525.

[7] Eshghinejadfard, A., 2017, "Lattice Boltzmann simulation of laminar and turbulent two-phase flows", Ph.D. thesis, Otto-von-Guericke-Universität Magdeburg.

[8] Uhlmann, M., 2005, "An immersed boundary method with direct forcing for the simulation of particulate flows", *Journal of Computational Physics*, Vol. 209 (2), pp. 448–476.

[9] Eshghinejadfard, A., and Thévenin, D., 2016, "Numerical simulation of heat transfer in particulate flows using a thermal immersed boundary lattice Boltzmann method", *International Journal of Heat and Fluid Flow*, Vol. 60, pp. 31–46.

[10] Peskin, C. S., 2002, "The immersed boundary method", *Acta Numerica*, Vol. 11, p. 479–517.

[11] Johnson, K. L., 1987, *Contact mechanics*, Cambridge university press.

[12] Mindlin, R. D., and Deresiewicz, H., 2021, "Elastic Spheres in Contact Under Varying Oblique Forces", *Journal of Applied Mechanics*, Vol. 20 (3), pp. 327–344.